J. Fluid Mech. (1998), *vol.* 366, *pp.* 259–287. Printed in the United Kingdom

Near-contact motion of surfactant-covered spherical drops

By VITTORIO CRISTINI, J. BŁAWZDZIEWICZ†, AND MICHAEL LOEWENBERG

[1]Department of Chemical Engineering, Yale University, New Haven, CT 06520-8286, USA

(Received 14 July 1997 and in revised form 12 February 1998)

A lubrication analysis is presented for the near-contact axisymmetric motion of spherical drops covered with an insoluble non-diffusing surfactant. Detailed results are presented for the surfactant distribution, the interfacial velocity, and the gap width between the drop surfaces. The effect of surfactant is characterized by a dimensionless force parameter: the external force normalized by Marangoni stresses. Critical values of the force parameter have been established for drop coalescence and separation. Surfactant-covered drops are stable to rapid coalescence for external forces less than $4\pi kTac_0$, where c_0 is the surfactant concentration at the edge of the near-contact region and a is the reduced drop radius.

For subcritical forces, the behaviour of surfactant-covered drops is described by two time scales: a fast time scale characteristic of near-contact motion between drops with clean interfaces and a slow time scale associated with rigid particles. The surfactant distribution evolves on the short time scale until Marangoni stresses approximately balance the external force. Supercritical values of the external force cannot be balanced; coalescence and separation occur on the fast time scale. The coalescence time normalized by the result for drops with clean interfaces is independent of the viscosity ratio and initial gap width.

Under subcritical force conditions, a universal long-time behaviour is attained on the slow time scale. At long times, the surfactant distribution scales with the near-contact region and the surface velocity is directed inward which impedes the drop approach and accelerates their separation compared to rigid particles. For drops pressed together with a sufficiently large subcritical force, a shrinking surfactant-free clean spot forms.

Surfactant-covered drops exhibit an elastic response to unsteady external forces because of energy stored in the surfactant distribution.

1. Introduction

The adsorption of surfactants at interfaces strongly affects the behaviour of emulsion drops. Convection of surfactant generates surface tension gradients that modify the stress balance on drop interfaces (Levich 1962). The complex nonlinear coupling of surfactant transport and fluid motion produce a wide range of phenomena that influence drop coalescence (Hodgson & Lee 1969), breakup (Stone & Leal 1990; Pawar & Stebe 1996), and macroscopic emulsion flows (Pal 1993; Li & Pozrikidis 1997).

† Institute of Fundamental Technological Research, Polish Academy of Sciences, Swiętokrzyska 21, 00-048 Warsaw, Poland.

Recent investigations are reviewed by Edwards, Brenner & Wasan (1991), Kralchevsky, Danov & Ivanov (1996), and Maldarelli & Huang (1996).

Many investigations have explored the effects of surfactant on the drainage of thin films (Kralchevsky *et al.* 1996; Ivanov 1988; see also references in Maldarelli & Huang 1996). Unfortunately, these analyses rely on *ad hoc* boundary and initial conditions to describe the near-contact motion and coalescence of emulsion drops. Yiantsios & Davis (1991) developed a description for the near-contact motion of slightly deformable drops that rigorously couples the initial and boundary conditions of the near-contact region to the outer flow. They considered fully mobile and tangentially immobilized interfaces but surfactant effects were ignored.

In the absence of van der Waals attraction, rigid particles are stable to aggregation but spherical drops with clean interfaces coalesce readily (Kim & Karrila 1991). Adsorbed surfactant reduces interfacial mobility which affects near-contact motion and may stabilize emulsion drops against coalescence; however, quantitative predictions are unavailable. The goal of this work is to provide a theoretical description of these phenomena for spherical surfactant-covered drops.

The assumptions of our analysis are stated in § 2. In § 3, the equations that describe the relative drop motion and the evolution of surfactant on the drop surfaces are derived. In § 4, a detailed analysis of the problem is presented and analytical results are derived. The results of numerical calculations are presented in § 5. Concluding remarks are given in § 6.

2. Assumptions

In this paper, we formulate a lubrication description for the axisymmetric near-contact motion between two undeformed spherical drops with reduced radius $a = a_1 a_2/(a_1 + a_2)$ that are separated by a small gap $h_0 \ll a$. The drop surfaces are covered by an insoluble non-diffusing surfactant with concentration c_0 at the edge of the near-contact region. The drops move with relative velocity U under the action of a prescribed external force F that arises from buoyancy or from an imposed flow field. The viscosity of the bulk fluid is μ and the viscosity of the drops is $\lambda\mu$.

Drop deformation becomes important when the dynamic pressure in the gap is comparable to the capillary pressure σ_0/a, where σ_0 is the surface tension evaluated at c_0. Herein, the dynamic pressure results from Marangoni stresses and therefore has the characteristic value $\Delta\sigma/h_0$, as shown in § 3.1, where $\Delta\sigma$ is the variation in surface tension on the interface in the near-contact region. Thus, drop deformation can be neglected only if $\Delta\sigma/\sigma_0 \ll h_0/a$. Our investigation was restricted to drops with a dilute coating of surfactant in order to explore the behaviour for $\Delta c/c_0 = O(1)$, where Δc is the variation of surfactant concentration in the near-contact region. The ideal equation of state is therefore appropriate:

$$\sigma(c) - \sigma(0) = -kTc, \tag{2.1}$$

where $\sigma(0)$ is the surface tension for clean interfaces, k is the Boltzmann constant and T is the temperature.

At small gap widths, van der Waals attraction becomes important and induces rapid coalescence. This occurs when the disjoining pressure becomes comparable to the dynamic pressure, $A/h_0^3 \sim \Delta\sigma/h_0$, where A is the Hamaker constant and $\Delta\sigma \sim kTc_0$. With $A \sim kT$ (e.g. Russel, Saville & Schowalter 1989), van der Waals attraction induces rapid coalescence for $h_0 < c_0^{-1/2}$. For dilute surfactant concentrations $c_0 = 10^{15}$ molecules/m^2 ($\approx 10^{-3}$ maximum coverage, e.g. Edwards *et al.* 1991) this corresponds

to gap widths less than 30 nm. Similarly, drop deformation becomes significant for $h_0 \leqslant kTc_0a/\sigma_0$. We conclude that the onset of coalescence precedes deformation for small drops with $a < \sigma_0/(kTc_0^{3/2})$. At room temperature with dilute surfactant concentrations and $\sigma_0 \approx 10^{-2}$ N m^{-1}, this criterion corresponds to sub-100 μm drops.

The diffusive flux of surfactant is $u_D c_0 = M\tau_v$, where M is the mobility of surfactant molecules, $\tau_v \sim \mu u/h_0$ is the viscous stress in the near-contact portion of the drop interfaces, and u is the interfacial velocity. Given $M \sim (\mu d)^{-1}$, where d is the effective hydrodynamic size of an adsorbed surfactant molecule, we conclude that surface diffusion becomes important when $u_D/u \sim (dh_0c_0)^{-1} = O(1)$. For dilute surfactant concentrations, and a hydrodynamic size of $d = 40$ nm which corresponds to a typical surface diffusivity 10^{-10} m^2 s^{-1} (e.g. Kralchevsky *et al.* 1996), we conclude that surface diffusion becomes significant only for gap widths less than 30 nm. At these very small gap widths, steric effects may arise from the finite size of adsorbed surfactant molecules.

Surfactant solubility is characterized by $c_0 = Kc_B$, where c_B is the bulk concentration and K is the adsorption constant which provides an estimate of the fluid layer that contains as much surfactant as adsorbed on the interface. For $K \gg h_0$ surfactant solubility in the continuous-phase fluid is unimportant.

For dilute surfactant concentrations, the effects of surface viscosity are unimportant and therefore ignored.

3. Problem statement

3.1. *Governing equations*

The fluid velocity v and pressure p in the near-contact region are described by the lubrication equations (Kim & Karrila 1991):

$$\mu\frac{\partial^2 v}{\partial z^2} = \frac{\partial p}{\partial x}, \tag{3.1}$$

$$2\pi x\int_0^h v\,\mathrm{d}z = \pi x^2 U, \tag{3.2}$$

where x, z are cylindrical coordinates with vertical coordinate z measured from the surface of a drop and radial coordinate x measured from the centre of the gap. The fluid velocity v is in the x−direction and

$$h = h_0 + \frac{x^2}{2a} \tag{3.3}$$

is the local gap width. The lateral extent of the near-contact region is $(ah_0)^{1/2}$. The gap width at $x = 0$ evolves according to

$$\dot{h_0} = -U, \tag{3.4}$$

Herein, the relative velocity U and the external force F are positive for drops that are pressed together and negative for drops that are pulled apart.

The fluid velocity is continuous across the interface. Thus, the flow drives a circulation inside the drops and convects surfactant on the drop interfaces. Gradients of surface tension (Marangoni stresses) arise and are balanced by the jump in

tangential viscous stresses across the interfaces at $z = 0$ and $z = h$:

$$\frac{\partial \sigma}{\partial x} = \left[-\mu \frac{\partial v}{\partial z} \right], \tag{3.5}$$

where $[g] = g(z^+) - g(z^-)$.

Under the assumptions that bulk solubility and surface diffusion are negligible, the conservation equation that describes the surfactant distribution is (Kralchevsky *et al.* 1996)

$$\frac{\partial c}{\partial t} = -\frac{1}{x} \frac{\partial (xuc)}{\partial x}. \tag{3.6}$$

The surfactant distribution satisfies the boundary conditions $c = c_0$ at $x \to \infty$ and $\partial c/\partial x = 0$ at $x = 0$. The interfacial velocity u and the surfactant concentration are nonlinearly coupled. Thus, a resistance formulation of the problem (specified relative velocity) is not simply related to a mobility formulation (specified force). Herein, we use a mobility formulation to find the relative motion of the drops under the action of a prescribed force.

Although the problem is nonlinear, the Stokes equations and the boundary conditions are linear for a given instantaneous distribution of surfactant. Thus, the fluid velocity can be decomposed into a velocity field resulting from the relative motion of drops with clean interfaces and a velocity field resulting from Marangoni stresses on the interfaces of stationary drops. The external force is balanced by a contribution from each of these velocity fields:

$$F = F_0 + F_M, \tag{3.7}$$

where F_M is the force generated by Marangoni stresses and

$$F_0 = 6\pi \mu a f U \tag{3.8}$$

is the lubrication force between drops with clean interfaces moving with relative velocity U. The coefficient f is the lubrication resistance.

For drops with clean interfaces, viscous stresses scale as $\mu u_p/h_0$ in the gap and $\mu u/(h_0 m)$ within the drops, where u_p is the magnitude of the pressure-driven parabolic flow in the gap, u is the tangential velocity on the drop interfaces, and $m = \lambda^{-1}\epsilon^{-1/2}$ is the interfacial mobility with dimensionless gap width, $\epsilon = h_0/a \ll 1$. By continuity of tangential stress, we have $u/u_p \approx m$ (Davis, Schonberg & Rallison 1989). Herein, $m \gg 1$ is assumed; surfactant effects are less important for highly viscous drops with $m \leqslant O(1)$ because the low interfacial mobility inhibits the generation of Marangoni stresses by displacement of surfactant. For $m \gg 1$, the velocity profile in the gap is approximately flat with $v = u$ and

$$u = \frac{xU}{2h}, \tag{3.9}$$

according to (3.2) with an error of $O(1/m)$. For $\epsilon^{1/2} \ll \lambda \ll \epsilon^{-1/2}$, the lubrication resistance is (Zinchenko 1982):

$$f = \frac{2^{1/2}\pi^2}{16\epsilon^{1/2}}\lambda + O(\log \epsilon). \tag{3.10}$$

For bubbles ($\lambda = 0$)

$$f = -\tfrac{1}{3}\log\epsilon + B, \tag{3.11}$$

where B depends on the size ratio; for equal-size bubbles, $B = 1.078$ (Kim & Karrila 1991). For drops, the lubrication resistance and the results obtained herein are independent of size ratio.

For stationary surfactant-covered drops, velocity gradients scale as u/h_0 in the gap as the result of the zero-net-flow constraint. Inside the drops, velocity gradients scale as $u/(ah_0)^{1/2}$. It follows that viscous stresses scale as $\mu u/h_0$ in the gap and $\mu\lambda u/(ah_0)^{1/2} = \mu u/(h_0 m)$ inside the drops. For $m \gg 1$, viscous stresses in the gap balance Marangoni stresses to $O(1/m)$ and (3.5) reduces to

$$kT\frac{\partial c}{\partial x} = -\mu\frac{\partial v}{\partial z} \tag{3.12}$$

at the surface $z = 0$, where the equation of state (2.1) has been inserted and v is the velocity field in the gap. The sign is changed for $z = h$.

For a given distribution of surfactant with $U = 0$, (3.1), (3.2), and (3.12) yield

$$\frac{\partial p}{\partial x} = -\frac{2kT}{h}\frac{\partial c}{\partial x} \tag{3.13}$$

and

$$v = \frac{kT}{\mu h}\frac{\partial c}{\partial x}\left[\frac{h^2}{12} - \left(z - \frac{h}{2}\right)^2\right]. \tag{3.14}$$

Equation (3.13) indicates that the dynamic pressure resulting from Marangoni stresses is $O(\Delta\sigma/h_0)$. It follows from (3.14) that the tangential velocity on the drop interfaces is

$$u = -\frac{hkT}{6\mu}\frac{\partial c}{\partial x}. \tag{3.15}$$

Given that $p = 0$ outside the near-contact region, the force generated by Marangoni stresses is

$$F_M = 2\pi\int_0^\infty xp\,\mathrm{d}x. \tag{3.16}$$

Integrating (3.13), inserting the resulting expression for p into (3.16), integrating by parts twice, and using the boundary condition $c \to c_0$ as $x \to \infty$, we obtain

$$F_M = 4\pi kTa\left[c_0 - \int_0^\infty c\frac{\partial}{\partial x}\left(1 - \frac{h_0}{h}\right)\mathrm{d}x\right]. \tag{3.17}$$

Neglecting the $O(1/m)$ internal viscous stresses in the derivation of (3.12) induces an error of the same magnitude in (3.17) which is therefore accurate to $O(\epsilon^{1/2})$ for $\lambda = O(1)$. For bubbles, the relative accuracy of (3.17) is $O(\epsilon\log\epsilon)$. F_0 and F_M are each accurate to leading order in m.

Inserting the net interfacial velocity,

$$u = \frac{xU}{2h} - \frac{hkT}{6\mu}\frac{\partial c}{\partial x}, \tag{3.18}$$

given by the linear superposition of (3.9) and (3.15) into (3.6) yields the evolution equation for the surfactant distribution:

$$\frac{\partial c}{\partial t} = -\frac{1}{x}\frac{\partial}{\partial x}\left[xc\left(\frac{Ux}{2h} - \frac{kTh}{6\mu}\frac{\partial c}{\partial x}\right)\right], \tag{3.19}$$

which satisfies the same boundary conditions as (3.6).

Equations (3.4), (3.7), (3.8), (3.17), and (3.19) form a closed set describing the near-contact motion of the drops, starting from an initial gap width and distribution of surfactant.

A pair of coupled evolution equations is obtained for the surfactant distributions on drop interfaces with different equilibrium concentrations c_1 and c_2:

$$\frac{\partial c_1}{\partial t} = -\frac{1}{x}\frac{\partial}{\partial x}\left[xc_1\left(\frac{Ux}{2h} - \frac{kTh}{3\mu}\frac{\partial c_1}{\partial x} + \frac{kTh}{6\mu}\frac{\partial c_2}{\partial x}\right)\right]. \tag{3.20}$$

$$\frac{\partial c_2}{\partial t} = -\frac{1}{x}\frac{\partial}{\partial x}\left[xc_2\left(\frac{Ux}{2h} - \frac{kTh}{3\mu}\frac{\partial c_2}{\partial x} + \frac{kTh}{6\mu}\frac{\partial c_1}{\partial x}\right)\right], \tag{3.21}$$

The force generated by Marangoni stresses is given by (3.17) with the substitution $c = \frac{1}{2}(c_1 + c_2)$.

3.2. *Dimensionless formulation*

In what follows, a constant external force is assumed. It is convenient to introduce the dimensionless variables

$$\epsilon = \frac{h_0}{a}; \quad y = 1 - \frac{h_0}{h}; \quad \bar{c} = \frac{c}{c_0}. \tag{3.22}$$

In these variables, the extent of the near-contact region is invariant and finite: $0 \leqslant y \leqslant 1$. The initial dimensionless gap is ϵ_0.

According to (3.17),

$$F_M \leqslant F_s, \tag{3.23}$$

where

$$F_s = 4\pi kTac_0. \tag{3.24}$$

We therefore introduce the dimensionless forces

$$\hat{F} = \frac{F}{F_s}, \quad \hat{F}_M = \frac{F_M}{F_s}. \tag{3.25}$$

There are two relevant velocity scales and two time scales for the problem:

$$U_p = \frac{F\epsilon}{6\pi\mu a}, \quad U_0 = \frac{F}{6\pi\mu af}; \tag{3.26}$$

$$\tau_p = 6\pi\mu a^2/|F|, \quad \tau_0 = \tfrac{3}{4}(2\epsilon_0)^{1/2}\pi^3 a^2\mu\lambda/|F|; \tag{3.27}$$

where U_p and U_0 are, respectively, the near-contact relative velocity between rigid particles and between drops with clean interfaces. The time scale τ_p (Stokes time) characterizes the near-contact motion between rigid particles and τ_0 is the coalescence time for drops with clean interfaces. For $m \gg 1$, the ratio of the time scales $\tau_p/\tau_0 = 4\sqrt{2\pi^{-2}m}$ is large.

In terms of the dimensionless variables, the interfacial velocity (3.18) becomes

$$\frac{u}{U} = \left(\frac{y(1-y)}{2\epsilon}\right)^{1/2} \left(1 - \frac{1}{2\hat{F}\bar{U}}\frac{\partial \bar{c}}{\partial y}\right) \tag{3.28}$$

and the equations of motion (3.4), (3.7), (3.8), (3.17), and (3.19) become

$$\mp \frac{1}{\epsilon}\frac{\mathrm{d}\epsilon}{\mathrm{d}\bar{t}} = \bar{U}, \tag{3.29}$$

$$\epsilon f \bar{U} = 1 - \frac{\hat{F}_M}{\hat{F}}, \tag{3.30}$$

$$\hat{F}_M = \int_0^1 (1-\bar{c})\mathrm{d}y, \tag{3.31}$$

and

$$\mp \frac{1}{\bar{U}}\frac{\partial \bar{c}}{\partial \bar{t}} = y(1-y)\frac{\partial \bar{c}}{\partial y} + (1-y)^2\left[\frac{\partial(\bar{c}y)}{\partial y} - \frac{1}{2\hat{F}\bar{U}}\frac{\partial}{\partial y}\left(\bar{c}y\frac{\partial \bar{c}}{\partial y}\right)\right], \tag{3.32}$$

where $\bar{t} = t/\tau_p$ and $\bar{U} = U/U_p$. At $y = 1$, we have $\bar{c} = 1$; the boundary condition $\partial\bar{c}/\partial x = 0$ at $x = 0$ is automatically enforced for $\partial\bar{c}/\partial y$ non-singular at $y = 0$. In (3.29) and (3.32), the minus sign applies for $\hat{F} > 0$ and the plus sign for $\hat{F} < 0$.

4. Analytical results

4.1. *Short-time behaviour*

According to (3.30) $\bar{U} \gg 1$ unless $F_M \approx F$. For a uniform initial distribution of surfactant, $F_M = 0$ at $t = 0$, thus $\bar{U} \gg 1$ for short times. According to (3.10), (3.11), and (3.30), $\hat{F}\bar{U} \sim \epsilon^{-1/2}$ for viscous drops and $\hat{F}\bar{U} \sim \epsilon^{-1}/\log\epsilon^{-1}$ for bubbles. Thus to leading order, (3.28) reduces to (3.9) indicating that the tangential velocity profile is unaffected by the surfactant distribution. Surfactant is passively convected; however, the non-uniform distribution of surfactant generates Marangoni stresses associated with the force F_M. For $m \gg 1$, the viscosity ratio merely sets the time scale for the short-time behaviour.

The nonlinear term in (3.32) is $O(\epsilon^{1/2})$ for drops and $O(\epsilon\log\epsilon)$ for bubbles. By neglecting this term, (3.32) reduces to a first-order linear equation. For a uniform initial distribution of surfactant c_0, the solution is

$$c = c_0 q, \tag{4.1}$$

where

$$q = \frac{\epsilon}{[\epsilon^2 + (\epsilon_0^2 - \epsilon^2)(1-y)^2]^{1/2}}. \tag{4.2}$$

For an arbitrary initial distribution of surfactant $c_0 g(y)$,

$$c = c_0\, q\, g\big(1 - (1-y)q\epsilon_0/\epsilon\big). \tag{4.3}$$

These results indicate that the surfactant concentration at the centre of the near-contact region varies linearly with the gap.

By inserting (4.3) into (3.31), we find the short-time approximation for the force generated by Marangoni stresses:

$$\hat{F}_{MS}(\epsilon) = \int_0^1 \big[1 - q\, g\big(1 - (1-y)q\epsilon_0/\epsilon\big)\big]\,\mathrm{d}y. \tag{4.4}$$

For a uniform initial distribution of surfactant,

$$\hat{F}_{MS} = 1 - \frac{\epsilon}{(\epsilon_0^2 - \epsilon^2)^{1/2}} \log \frac{\epsilon}{\epsilon_0 - (\epsilon_0^2 - \epsilon^2)^{1/2}}, \quad \epsilon \leqslant \epsilon_0, \tag{4.5}$$

$$\hat{F}_{MS} = 1 - \frac{\epsilon}{(\epsilon^2 - \epsilon_0^2)^{1/2}} \arcsin \frac{(\epsilon^2 - \epsilon_0^2)^{1/2}}{\epsilon}, \quad \epsilon \geqslant \epsilon_0, \tag{4.6}$$

which reduce to a linear dependence on gap width for small displacements:

$$\hat{F}_{MS} = \frac{1}{3}\left(1 - \frac{\epsilon}{\epsilon_0}\right) + O\left(1 - \frac{\epsilon}{\epsilon_0}\right)^2, \quad \epsilon/\epsilon_0 \approx 1. \tag{4.7}$$

The force generated by Marangoni stresses is monotonic in gap width and has the limiting values

$$\hat{F}_{MS} = 1 + \frac{\epsilon}{\epsilon_0} \log \frac{\epsilon}{2\epsilon_0} + O(\epsilon/\epsilon_0)^3, \quad \epsilon/\epsilon_0 \ll 1, \tag{4.8}$$

$$\hat{F}_{MS} = 1 - \frac{\pi}{2} + \frac{\epsilon_0}{\epsilon} + O(\epsilon_0/\epsilon)^2, \quad \epsilon/\epsilon_0 \gg 1. \tag{4.9}$$

The short-time near-contact velocity of the drops is obtained by inserting $\hat{F}_M = \hat{F}_{MS}$ into (3.30).

By integrating (3.30) with (3.10) for viscous drops we obtain

$$t(\epsilon) = \pm\tau_0 \int_{\epsilon/\epsilon_0}^{1} \frac{\hat{F}}{\hat{F} - \hat{F}_{MS}(\epsilon_0 s)} \, \mathrm{d}s^{1/2}. \tag{4.10}$$

The plus sign applies for $\hat{F} > 0$ and the minus sign for $\hat{F} < 0$. For bubbles the corresponding formula is obtained using (3.11).

4.1.1. *Critical values of force*

From the general upper bound (3.23), supercritical external forces $\hat{F} > 1$ cannot be balanced by Marangoni stresses. The limiting formula (4.8) for a uniform initial distribution of surfactant is consistent with this general prediction. According to (4.10), $t(0) \leqslant \tau_0 \hat{F}/(\hat{F} - 1)$. Thus for $\hat{F} > 1$, coalescence occurs on the times scale τ_0 for any initial surfactant distribution.

No general lower bound exists for the force generated by Marangoni stresses when drops are pulled apart by an external force. For a uniform initial distribution of surfactant, the drops separate on the time scale τ_0 for supercritical pulling forces $\hat{F} < 1 - \frac{1}{2}\pi$, according to (4.9)–(4.10). A complementary result for $\hat{F} < 1 - \frac{1}{2}\pi$ is obtained from the long-time behaviour in § 4.2.2.

Equation (4.10) indicates that for subcritical values of the external force

$$1 - \tfrac{1}{2}\pi < \hat{F} < 1, \tag{4.11}$$

the force balance

$$\hat{F}_{MS}(\epsilon_s) = \hat{F} \tag{4.12}$$

is established at $\epsilon = \epsilon_s$. Equation (3.30) yields $U/U_0 \approx 0$ at $\epsilon = \epsilon_s$, provided that $\hat{F}_M \approx \hat{F}_{MS}$. According to the analysis presented in § 4.2, the stable gap ϵ_s corresponds to the transition from rapid gap evolution on the short time scale τ_0 to slow evolution on the long time scale $\tau_p \gg \tau_0$.

For a uniform initial distribution of surfactant, the stable gap width is determined by (4.5) and (4.6). The asymptotic formulae (4.8) and (4.9) indicate that the stable gap vanishes for $\hat{F} \to 1$ and diverges for $\hat{F} \to 1 - \frac{1}{2}\pi$.

4.1.2. *Rapid coalescence*

For $\hat{F} > 1$, the entire evolution is well described by the short-time equations. For drops, the coalescence time

$$\tau = t(0) \tag{4.13}$$

can be accurately estimated from (4.10). Thus, τ scales with τ_0 and τ/τ_0 is independent of the initial gap and the viscosity ratio.

For a uniform initial surfactant distribution $F_M \geqslant 0$, thus $\tau \geqslant \tau_0$, according to (3.30). An analysis of (4.10) indicates that $\tau \approx \tau_0$ for a large external force:

$$\frac{\tau}{\tau_0} = 1 + 0.4897\hat{F}^{-1} + 0.3407\hat{F}^{-2} + O(\hat{F}^{-3}), \quad \hat{F} \gg 1, \tag{4.14}$$

and that τ diverges for a near-critical force:

$$\frac{\tau}{\tau_0} = \frac{\pi}{2}\frac{1}{[-(\hat{F}-1)\log(\hat{F}-1)]^{1/2}} + O(\hat{F}-1), \quad \hat{F} \to 1. \tag{4.15}$$

The formula for bubbles corresponding to (4.10) depends on the initial gap and and size ratio. For bubbles, $\tau/\tau_0 \sim -\log(\hat{F}-1)$ for $\hat{F} \to 1$.

4.2. *Long-time stable behaviour*

4.2.1. *Governing equations*

For subcritical values (4.11) of the external force the hydrodynamic force induced by the Marangoni stresses approximately balances the external force at long times,

$$\hat{F} \approx \hat{F}_M, \tag{4.16}$$

and the interparticle velocity is significantly reduced according to the discussion in § 4.1.1. In this regime, (3.30) and (3.31) can be replaced by

$$\hat{F} = \int_0^1 (1-\bar{c})\mathrm{d}y, \tag{4.17}$$

and evolution of the surfactant distribution is described by (3.32) with $\bar{U}$ determined by (4.17). The gap width does not enter the long-time equations (3.32) and (4.17) but is determined by (3.29). The long-time evolution is independent of the viscosity ratio and initial gap width.

To determine the relative velocity $\bar{U}$ and examine the stability of the long-time solution, we calculate the rate of change of $\hat{F}_M$ by integrating both sides of (3.32) with respect to y and inserting (3.31):

$$\pm\frac{\mathrm{d}\hat{F}_M}{\mathrm{d}\bar{t}} = I_1\,\bar{U} - \frac{I_2}{\hat{F}}, \tag{4.18}$$

where

$$I_1 = \int_0^1 \left[1-2(1-y)^2\right]\bar{c}\,\mathrm{d}y, \quad I_2 = \int_0^1 (y-\tfrac{1}{2})\bar{c}^2\,\mathrm{d}y. \tag{4.19}$$

For constant $\hat{F}$, (4.16) and (4.18) yield

$$\bar{U} = \frac{I_2}{I_1\hat{F}}. \tag{4.20}$$

It follows that $\bar{U} = O(1)$ and the long-time evolution is on the rigid-particle time scale τ_p except for unusual surfactant distributions with $I_1 \approx 0$ or for $I_2/\hat{F} \gg 1$.

Evolution with $\hat{F} \ll 1$ generates $\bar{c}(y) \approx 1$ so that $I_2/\hat{F} = O(1)$; relaxation processes with $I_2/\hat{F} \gg 1$ are discussed in § 4.3.1.

For $\bar{U} = O(1)$, equation (3.29) indicates that $t/\tau_p = O(\log(\epsilon/\epsilon_0))$. Thus, drops that are pushed together by an external force $\hat{F} < 1$ do not coalesce; however, drop separation occurs in a finite time whether or not the critical pulling force is exceeded.

For $\hat{F} > 0$ and $\bar{c}(y)$ an increasing function of y (e.g. $\bar{c}$ resulting from the short-time evolution) (4.19) and (4.20) imply that $\bar{U} > 0$. For $\hat{F} < 0$ and $\bar{c}(y)$ decreasing, $\bar{U} > 0$ provided that $I_1 > 0$.

The stability of the long-time force balance (4.16) is analysed by considering the relation obtained from (3.30) and (4.18):

$$\pm \hat{F} \frac{\mathrm{d}}{\mathrm{d}\bar{t}}(\epsilon f \bar{U}) = -I_1 \bar{U} + \frac{I_2}{\hat{F}}. \tag{4.21}$$

Inserting expansions around the long-time solutions,

$$\bar{c} = \bar{c}_L + \delta\bar{c}, \qquad \bar{U} = \bar{U}_L + \delta\bar{U}, \tag{4.22}$$

into (4.21) yields

$$\pm \left[\hat{F} \frac{\mathrm{d}}{\mathrm{d}\bar{t}} \left(\epsilon f \bar{U}_L \right) + \hat{F} \frac{\mathrm{d}}{\mathrm{d}\bar{t}} \left(\epsilon f \delta\bar{U} \right) \right] = -I_1(\bar{c}_L)\delta\bar{U} - I_1(\delta\bar{c})\bar{U}_L + \frac{I_2(\delta\bar{c})}{\hat{F}}, \tag{4.23}$$

where unperturbed quantities on the right-hand side have been eliminated by (4.20). We consider $\delta\bar{c}$ orthogonal to perturbations with $\int_0^1 \delta\bar{c}\,\mathrm{d}y = 0$ because only these affect the force balance. Equation (4.23) simplifies because $\mathrm{d}(\epsilon f)/\mathrm{d}\bar{t} \sim \epsilon^{1/2}$ according to (3.29) and $\delta\bar{c} \sim \epsilon^{1/2}\bar{U}_L$ according to (3.30) and (3.31). Thus, at leading order

$$\pm \hat{F} \epsilon f \frac{\mathrm{d}}{\mathrm{d}\bar{t}} \delta\bar{U} = -I_1(\bar{c}_L)\delta\bar{U}. \tag{4.24}$$

The result indicates that perturbation $\delta\bar{U}$ decay on the time scale τ_0 and the long-time force balance (4.16) is restored provided that

$$I_1(\bar{c}_L) > 0. \tag{4.25}$$

The polynomial of the integrand in I_1, (4.19), changes sign within the integration domain, thus condition (4.25) is not guaranteed. However, it is satisfied for distributions with reduced concentrations at the centre of the near-contact region, such as those that result from the short-time approach of the drops. For a sufficiently small increase of the concentration at the centre of the near-contact region condition (4.25) is also satisfied.

With $\bar{U} = O(1)$, relation (4.16) is accurate to $O(\epsilon^{1/2})$ for viscous drops, as indicated by (3.30) and (3.31). For bubbles, (4.16) is accurate to $O(\epsilon \log \epsilon)$. Thus, according to the discussion below (3.17), expressions (3.31) and (4.17) have errors of the same order. It follows that the long-time approximation (3.29), (3.32), and (4.17) is accurate to the same order as the full description.

4.2.2. *Similarity solution*

On the assumption that the long-time solution tends to a self-similar form, a time-independent solution of (3.32) is sought. After introducing the change of variable,

$$C = \frac{\bar{c}}{4\bar{U}\hat{F}}, \tag{4.26}$$

(3.32) is independent of $\hat{F}$ and $\bar{U}$:

$$0 = y\frac{dC}{dy} + (1-y)\left[\frac{d(Cy)}{dy} - 2\frac{d}{dy}\left(Cy\frac{dC}{dy}\right)\right]. \tag{4.27}$$

The concentration profile is obtained by the normalization $\bar{c}(y) = C(y)/C(1)$, the force from (4.17), and the interfacial velocity is obtained from (3.28). According to (4.26),

$$\bar{U} = \frac{1}{4\hat{F}C(1)}, \tag{4.28}$$

and the rescaled concentration C has the same sign as $\hat{F}$.

Expanding $C(y)$ in a power series around $y = 0$ and inserting into (4.27) yields

$$C(y) = C(0) + \tfrac{1}{2}y + O(y^2), \quad y \to 0. \tag{4.29}$$

For a sufficiently strong subcritical pushing force, a clean spot forms on the drop interfaces with $C = 0$ for $y \leqslant y_0$. A power series expansion around $y = y_0$ yields

$$C(y) = \frac{1 - \frac{1}{2}y_0}{1 - y_0}(y - y_0) + O(y - y_0)^2, \quad y \to y_0. \tag{4.30}$$

The concentration profile is non-analytic around $y = 1$:

$$C(1) - C(y) \sim (1-y)^{\alpha}, \quad y \to 1, \tag{4.31}$$

where $\alpha = 1 - (2C(1))^{-1}$. Except for $\hat{F} \approx 1$, the radius of convergence for these expansions is less than unity, precluding the possibility of a single series expansion for the concentration profile on the entire domain: $0 \leqslant y \leqslant 1$.

According to (4.26), $|C| \gg 1$ for small external forces. A perturbation solution for $|\hat{F}| \ll 1$ is obtained from an expansion of $C(y)$ in powers of $1/C(0)$:

$$C(y) = C(0) + C_1(y) + \frac{1}{C(0)}C_2(y) + O\left(\frac{1}{C(0)}\right)^2. \tag{4.32}$$

Inserting (4.32) into (4.27) yields

$$C_1(y) = \tfrac{1}{2}y, \tag{4.33}$$

$$C_2(y) = -\frac{1}{4}\left[y + \int_0^y t^{-1}\log(1-t)\,dt\right], \tag{4.34}$$

and $C_2(1) = -1/4 + \pi^2/24$. Then from (4.17) and (4.28) we find that

$$\bar{U} = 1 - 2\hat{F} + O(\hat{F}^2) \tag{4.35}$$

and

$$\bar{c}(0) = 1 - 2\hat{F} + O(\hat{F}^2). \tag{4.36}$$

Equation (4.35) indicates that rigid-particle lubrication is recovered in the small force limit.

For $\hat{F} \to 1$, $y_0 \to 1$ which is consistent with (4.17) and (4.30). Combining (4.30) and (4.31) by enforcing $C(y_0) = 0$ and matching the derivative at $y = y_0$ yields

$$C(y) = 1 - \left(\frac{1-y}{1-y_0}\right)^{1/2} + O(1-y). \tag{4.37}$$

This result together with (4.28) indicates that for $\hat{F} \to 1$, the long-time relative velocity of the drops is considerably less than that for rigid particles:

$$\bar{U} = \tfrac{1}{4} + O(1 - \hat{F}). \tag{4.38}$$

A matched asymptotic expansion of the long-time similarity solution is derived in Appendix A for a near-critical pulling force. The asymptotic formula (A 10) and (4.28) indicate that $\bar{U}$ diverges for $|C(0)| \to 0$. Thus, according to (A 12) and (A 20), the critical pulling force for surfactant-covered drops is

$$\hat{F} = 1 - \tfrac{1}{2}\pi. \tag{4.39}$$

For $\hat{F}$ below this critical value, the long-time similarity solution cannot be attained for any initial distribution of surfactant. The same critical value was obtained from the short-time approximation in § 4.1. This coincidence follows from the fact that (4.2) equals the leading-order outer solution (A 4) of the long-time similarity equation in the limit $\epsilon/\epsilon_0 \to \infty$.

The relative velocity of the drops in the limit of critical pulling force is obtained by inserting relations (A 10), (A 12), and (A 22) into (4.28), which yields

$$\bar{U} = \frac{1}{a_0\,(2\pi - 4)\, f_s(\Delta\hat{F})}, \tag{4.40}$$

where $\Delta\hat{F} = \hat{F} - 1 + \frac{1}{2}\pi$, a_0 is given by (A 9), and $f_s(\Delta\hat{F})$ is obtained by inverting (A 20). Inserting the first-order iterative solution (A 23) yields

$$\bar{U} = \frac{-\log \Delta\hat{F} + \frac{9}{2} b/a_0}{9\,(\pi - 2)\,\Delta\hat{F}}, \tag{4.41}$$

where b is given by (A 21). Thus, $\bar{U}$ diverges as the critical pulling force is attained.

Combining (4.28), (4.40), (A 10), and (A 12) yields a relation between the external force and the surfactant concentration at the centre of the near-contact region:

$$\bar{c}(0) = \frac{1}{a_0 \left[f_s(\Delta\hat{F}) \right]^{1/3}}. \tag{4.42}$$

The divergence of $\bar{c}(0)$ at $\hat{F} \to 1 - \frac{1}{2}\pi$ is weaker than the divergence of $\bar{U}$.

The asymptotic formulae (4.40) and (4.42) can be combined with the expansions (4.35) and (4.36) to construct two-point approximations for $\bar{U}$ and $\bar{c}$, as discussed in Appendix B.

Equation (4.27) can be rearranged to yield

$$\frac{\mathrm{d}^2 C}{\mathrm{d}y^2} = \frac{1}{2y(1-y)} \left\{ 2 \left(\frac{1}{2} - \frac{\mathrm{d}C}{\mathrm{d}y} \right) (1-y) + \frac{y}{C} \frac{\mathrm{d}C}{\mathrm{d}y} \left[2 \left(\frac{1}{2} - \frac{\mathrm{d}C}{\mathrm{d}y} \right) (1-y) + 1 \right] \right\}. \tag{4.43}$$

The result indicates that $\mathrm{d}^2C/\mathrm{d}y^2 = [4C(1-y)]^{-1}$ for $\mathrm{d}C/\mathrm{d}y = \frac{1}{2}$ and $\mathrm{d}^2C/\mathrm{d}y^2 = [2y]^{-1}$ for $\mathrm{d}C/\mathrm{d}y = 0$. Given the initial conditions (4.29) or (4.30), it follows that

$$\frac{\mathrm{d}C}{\mathrm{d}y} \geqslant \frac{1}{2}, \quad y_0 \leqslant y \leqslant 1, \quad \hat{F} > 0, \tag{4.44}$$

where $y_0 \geqslant 0$ and

$$0 < \frac{\mathrm{d}C}{\mathrm{d}y} \leqslant \frac{1}{2}, \quad 0 \leqslant y \leqslant 1, \quad \hat{F} < 0. \tag{4.45}$$

According to (3.28), these results and definition (4.26) imply that

$$u(y) \leqslant 0, \quad y_0 \leqslant y \leqslant 1. \tag{4.46}$$

Surfactant backflow occurs because the long-time self-similar concentration profile scales with the size of the lubrication region. Surfactant backflow impedes the approach of surfactant-covered drops and accelerates their separation.

4.3. *External force fluctuations*

The foregoing analyses can be generalized to variable external force conditions; two examples are considered below.

4.3.1. *Relaxation*

During near-contact motion, energy is stored in the non-uniform surfactant distribution. To explore the reversibility of the drop motion, we consider a time-dependent external force:

$$\left.\begin{aligned} \hat{F}(t) &= \hat{F}, \quad -t_R < t \leqslant 0, \\ \hat{F}(t) &= 0, \quad t > 0, \end{aligned}\right\} \tag{4.47}$$

with a uniform surfactant distribution at $t = -t_R$. For $F = 0$, the long and short time scales are based on the characteristic Marangoni stress:

$$\tau_{sp} = 6\pi\mu a^2/F_s, \quad \tau_{s0} = \tfrac{3}{4}(2\epsilon_0)^{1/2}\pi^3 a^2 \mu\lambda/F_s, \tag{4.48}$$

where ϵ_0 is the gap width at $t = 0$ and F_s is given by (3.24). For $t = O(\tau_{s0})$, the relaxation process is described by the short-time equations with the initial surfactant distribution given at $t = 0$. The gap width evolves according to (4.10) which, for $\hat{F} = 0$, reduces to

$$t(\epsilon) = \tau_{s0} \int_1^{\epsilon/\epsilon_0} \frac{1}{\hat{F}_{MS}}\, \mathrm{d}s^{1/2}. \tag{4.49}$$

According to (4.12), the short-time relaxation continues until

$$\hat{F}_{MS}(\epsilon) = 0. \tag{4.50}$$

The entire relaxation process is characterized by short-time behaviour if the surfactant distribution at $t = 0$ corresponds to the distribution obtained by short-time evolution of a uniform profile, (4.1)–(4.2). In this case, the surfactant distribution evolves backwards to a uniform profile and final gap width $\epsilon = \epsilon_R$, where ϵ_R is the gap width at $t = -t_R$. Thus, for rapid displacements ($t_R \ll \tau_p$), the evolution of surfactant-covered drops is reversible and the behaviour is analogous to a damped nonlinear spring. For small displacements, $\epsilon_R - \epsilon$ decays exponentially with time constant $\frac{3}{2}\tau_{s0}$ according to (4.49) and (4.7).

For general surfactant distributions, the short-time relaxation is followed by a slower long-time relaxation on the time scale τ_{sp} which is characterized by $\hat{F}_M \approx \hat{F} = 0$. According to the discussion in § 4.2.1, the long-time evolution is described by (3.29) and (3.32) (with t and U rescaled using F_s instead of F) and the condition

$$\int_0^1 (1 - \bar{c})\, \mathrm{d}y = 0. \tag{4.51}$$

The long-time relative velocity given by (4.20) becomes

$$\frac{U}{U_{sp}} = \frac{I_2}{I_1}, \tag{4.52}$$

where $U_{sp} = \epsilon F_s/(6\pi\mu a)$. The result indicates that $U/U_{sp} = O(1)$ except for $I_1 \approx 0$.

4.3.2. *Small force fluctuations*

At long times, Marangoni stresses balance the external force. The initial response to an external force fluctuation

$$\left.\begin{aligned} \hat{F}(t) &= \hat{F}, \quad -t_R < t \leqslant 0, \\ \hat{F}(t) &= \hat{F} + \delta\hat{F}, \quad t > 0 \end{aligned}\right\} \tag{4.53}$$

is described by the short-time solution. The stable gap width ϵ_s and surfactant distribution adjust on the time scale τ_0 until the external force is again balanced by Marangoni stresses. By inserting $\epsilon = \epsilon_0 + \delta\epsilon$ and (4.53) into (4.1)–(4.4) and (4.12), we obtain

$$-\frac{1}{\epsilon_0}\frac{\delta\epsilon}{\delta\hat{F}} = \frac{1}{I_1}, \tag{4.54}$$

where I_1 is given by (4.19) with $\bar{c}(y)$ corresponding to a long-time surfactant distribution for $\hat{F}$. This result can also be derived from (4.18) by inserting (3.29) and neglecting $I_2/\hat{F}$ consistent with the short-time approximation. For $I_1 > 0$, (4.54) describes short-time adjustment of the gap; for $I_1 < 0$, the long-time solution is unstable, according to (4.25).

The result (4.54) requires only that (4.16) applies; it is not necessary that the long-time similarity solution be attained. If the long-time similarity solution is established, we obtain the asymptotic formulae

$$-\frac{1}{\epsilon_0}\frac{\delta\epsilon}{\delta\hat{F}} = 3 + \tfrac{10}{3}\hat{F}^2 + O(\hat{F})^3, \quad \hat{F} \ll 1, \tag{4.55}$$

$$-\frac{1}{\epsilon_0}\frac{\delta\epsilon}{\delta\hat{F}} = \frac{1}{1-\hat{F}} + O(1), \quad \hat{F} \to 1, \tag{4.56}$$

from (4.26), (4.32), and (4.37) and

$$-\frac{1}{\epsilon_0}\frac{\delta\epsilon}{\delta\hat{F}} = \frac{1}{3\Delta\hat{F} + (b_1 - 3b)f_s(\Delta\hat{F})} + O(1), \quad \hat{F} \to 1 - \tfrac{1}{2}\pi, \tag{4.57}$$

using (A 20), (A 22), and (A 26) with b and b_1 given by (A 21) and (A 27). For $\hat{F}$ close to the critical values, (4.56)–(4.57) indicate that the stable gap width is very sensitive to small fluctuations in the external force. The asymptotic formulae (4.55) and (4.57) can be combined to yield a two-point approximation, as discussed in Appendix B.

5. Numerical results

Equations (3.29)–(3.32) were numerically integrated using fixed collocation points in the dimensionless variable y. The resulting set of first-order ordinary differential equations is stiff; a backwards differentiation algorithm was used for time stepping (Hall & Watt 1976). Spatial derivatives of the surfactant concentration were evaluated using a cubic spline. The initial surfactant distribution $\bar{c}(y, 0)$ and initial gap width ϵ_0 are needed to fully specify the problem for given values of the parameters $\hat{F}$ and λ.

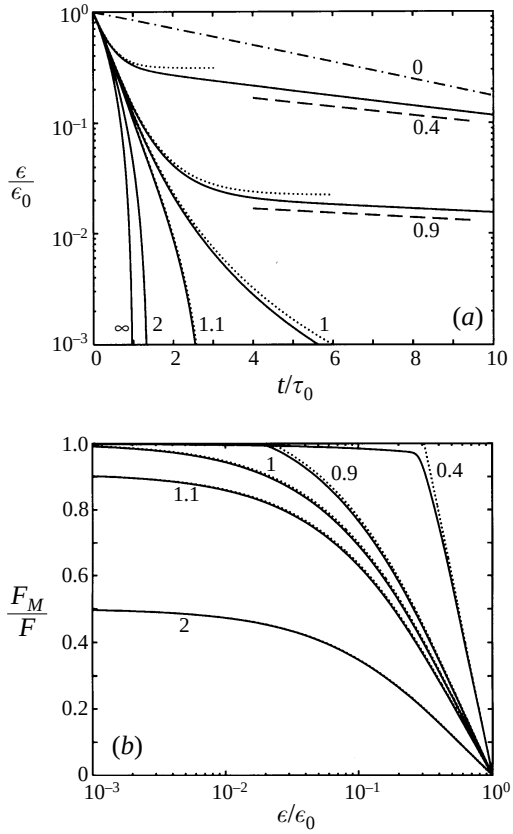

FIGURE 1. (*a*) Gap width history and (*b*) Marangoni force $\hat{F}_M$ versus gap width for drops pushed together with different values of $\hat{F}$ (as labelled); uniform initial distribution of surfactant, $\epsilon_0 = 0.01$, and $\lambda = 1$ (under these conditions, $\tau_p/\tau_0 = 5.73$): numerical solution (solid curves), short-time approximation (4.5)–(4.6) and (4.10) (dotted curves), slopes of long-time solution (dashed lines), rigid particle formula (dashed-dotted line).

The long-time similarity solution was obtained by numerical integration of (4.27) as an initial value problem with initial condition (4.29) or (4.30).

5.1. *Evolution of gap width and Marangoni stresses*

The gap width history for drops pushed together by a constant force is depicted in figure 1 (*a*). The Marangoni force is shown as a function of gap width in figure 1 (*b*). The corresponding results for drops that are pulled apart are shown in figure 2.

Two distinct behaviours are observed, corresponding to sub- and supercritical values of the external force $\hat{F}$. For supercritical values $\hat{F} > 1$, the drops coalesce on the time scale τ_0, the coalescence time for drops with clean interfaces; for drops pulled apart with $\hat{F} < 1 - \frac{1}{2}\pi$, the drops separate on this time scale. For subcritical values $1 - \frac{1}{2}\pi < \hat{F} < 1$, the results show a transition from a short- to a stable long-time behaviour at $t \approx \tau_0$.

In agreement with the analysis presented in § 4.1, the system evolves on the time scale τ_0 as long as the external force $\hat{F}$ is not balanced by $\hat{F}_M$, the force generated by Marangoni stresses. If, in addition $t \ll \tau_p$, the evolution is accurately described by the short-time approximation.

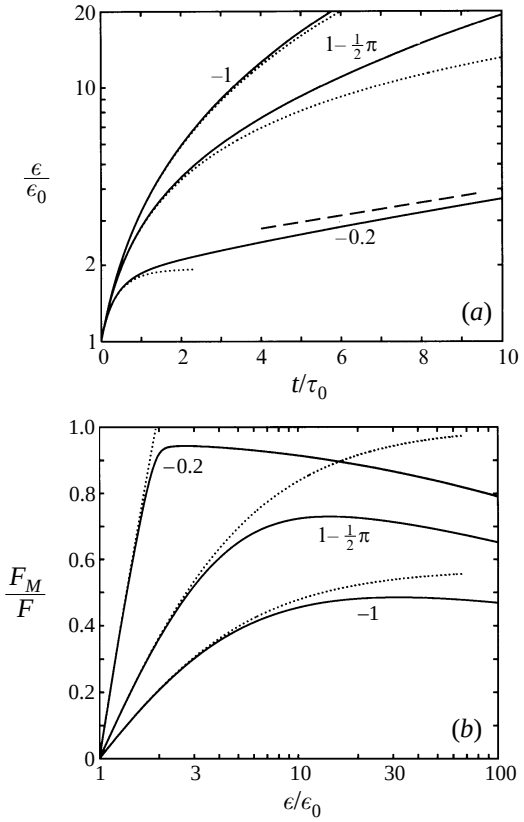

FIGURE 2. Same as figure 1 but for drops pulled apart, with $\epsilon_0 = 0.0005$ ($\tau_p/\tau_0 = 25.6$).

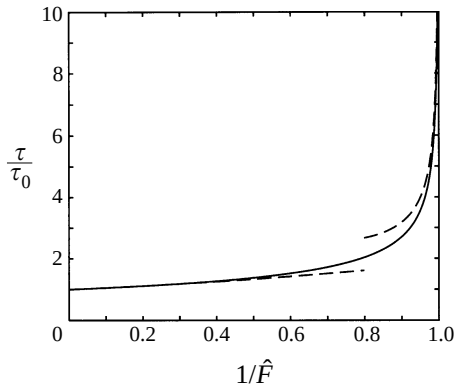

FIGURE 3. Drop coalescence time versus $1/\hat{F}$; uniform initial distribution of surfactant: results from short-time solution (4.13) (solid curve), asymptotic formulae (4.14) and (4.15) (dashed curves).

For supercritical force $\hat{F} > 1$, the results shown in figure 1(*a*) indicate that the short-time approximation is indistinguishable from the numerical solution, except for $\hat{F}$ very close to 1. Thus, the coalescence time is accurately predicted by the short-time approximation (4.13) shown in figure 3. The results indicate that drop coalescence time is weakly affected by surfactant for $1/\hat{F} < 0.8$ but diverges for $\hat{F} \to 1$.

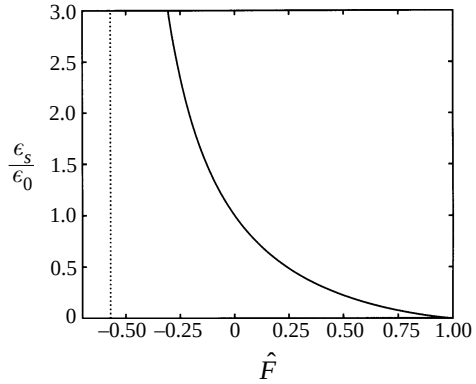

FIGURE 4. Stable gap defined by (4.12) versus force parameter (solid curve), critical pulling force (dotted line); uniform initial distribution of surfactant.

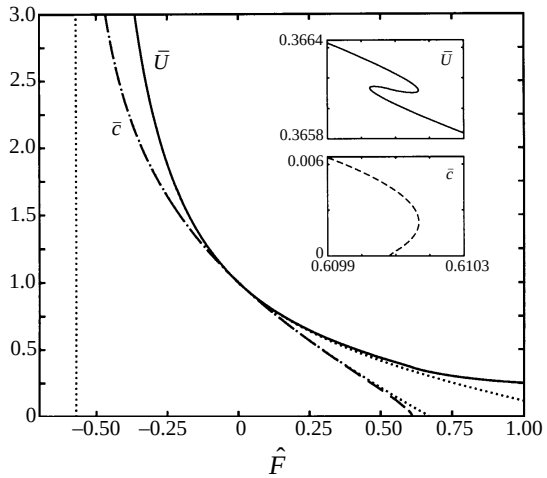

FIGURE 5. Long-time similarity solution for relative drop velocity $\bar{U} = U/U_p$ (solid curve) and surfactant concentration at centre of near-contact region $\bar{c}(0) = c(0)/c_0$ (dashed curve) versus force parameter; approximations described in Appendix B (dotted curves). Insets show behaviour for $\hat{F} \approx 0.61$.

For $1 - \frac{1}{2}\pi < \hat{F} < 1$, the results presented in figures 1 and 2 indicate that, to within the $O(\epsilon^{1/2})$ accuracy of our analysis, a balance between Marangoni stresses and the external force is achieved on the time scale τ_0, when the transition to the long-time behaviour occurs. For drops that are pulled apart, the force balance is gradually lost with increasing gap width, consistent with our analysis. A comparison of the short-time and numerical solutions presented in figures 1 and 2 indicate that the stable gap width corresponding to the transition is accurately predicted (4.12). The stable gap width ϵ_s is depicted in figure 4. As predicted by (4.8)–(4.9), ϵ_s vanishes at the critical pushing force and diverges at the critical pulling force.

In § 4.2.2 it was assumed that after the force balance (4.16) is established, the system evolves on the long time scale τ_p towards the similarity solution. The results in figures 1 and 2 support this assumption. In figure 5, the relative drop velocity obtained from the long-time similarity solution is shown as a function of $\hat{F}$. In agreement with the result of § 4.2.2, the long-time drop velocity is smaller than the corresponding particle

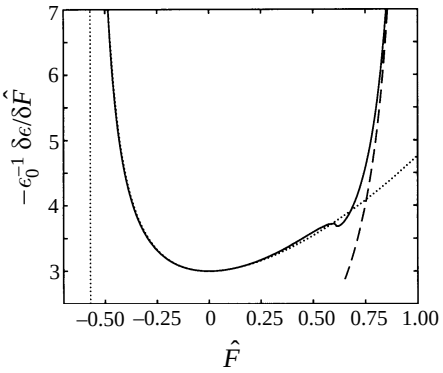

FIGURE 6. Sensitivity of gap width to force fluctuations versus $\hat{F}$; obtained from (4.54) for long-time similarity solution (solid curve), approximation described in Appendix B (dotted curve), and asymptotic formula (4.56) (dashed curve).

velocity for $\hat{F} > 0$ and is larger for $\hat{F} < 0$. Also shown is the surfactant concentration at the centre of the near-contact region. The two-point approximations described in Appendix B are accurate within their range of validity.

The results shown in figure 5 indicate that a clean spot forms in the near-contact region for $\hat{F} > 0.61$. A clean spot on an isolated sedimenting drop forms for $\hat{F} > 1$. This example illustrates that variations of surfactant concentration in the near-contact region and the outer region of the interface are generally both $O(\hat{F})$.

The inset shows that concentration and velocity exhibit hysteretic behaviour in a minute parameter range at the onset of clean spot formation. The stability of the long-time force balance was shown in § 4.2.1; however, the similarity solution apparently has an instability that evolves on the time scale τ_p for the parameter range shown in the inset of figure 5.

The response of the long-time similarity solution to fluctuations in the external force was obtained by inserting the corresponding concentration profile into (4.54). The results shown in figure 6 indicate that the solution becomes very sensitive to fluctuations in the external force near the critical values for $\hat{F}$. The increased sensitivity for $\hat{F} > 0.61$ corresponds to the formation of a clean spot in the near-contact region.

5.2. *Surfactant concentration and interfacial velocity profiles*

5.2.1. *Supercritical force*

Drop coalescence and separation occur on the short time scale τ_0 for supercritical values of the force parameter. Surfactant concentration profiles are depicted in figure 7 for the critical values $\hat{F} = 1$ and $\hat{F} = 1 - \frac{1}{2}\pi$; initially, the surfactant concentration is uniform.

The results depicted in figure 7 (*a*) indicate that the surfactant distribution broadens continuously on the length scale of the lubrication region when the drops are pressed together. At contact, surfactant is completely displaced from the near-contact region. When the drops are pulled apart, surfactant accumulates in the near-contact region, as illustrated in figure 7 (*b*).

Initially, the short-time approximation agrees with the numerical calculations as shown in figure 7. The interfacial velocity profile (not shown) is accurately described by (3.9) corresponding to plug flow in the gap. According to the short-time approximation, the surfactant concentration $\bar{c}$ at $x = 0$ equals the normalized gap width

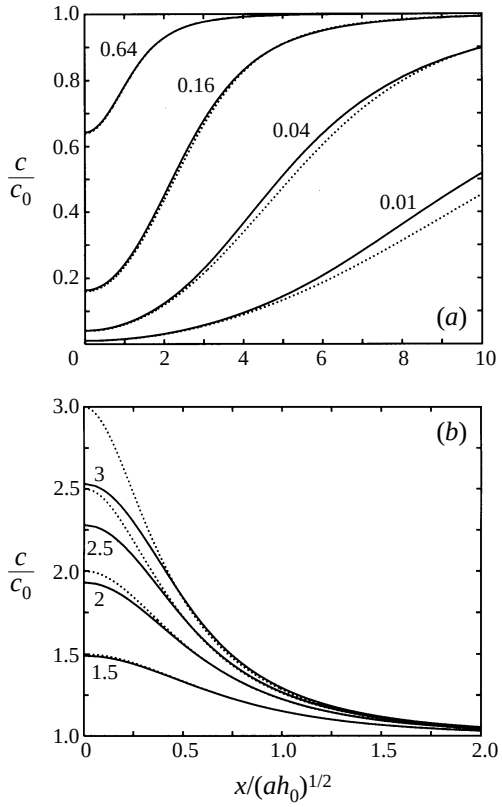

FIGURE 7. Surfactant concentration profiles at different gap widths ϵ/ϵ_0 (as labelled); with uniform initial distribution of surfactant: (*a*) $\hat{F} = 1$, $\epsilon_0 = 0.01$; (*b*) $\hat{F} = 1 - \frac{1}{2}\pi$, $\epsilon_0 = 0.0005$. Numerical results for $\lambda = 1$ (solid curves), short-time approximation (4.1)–(4.2) (dashed curves).

ϵ/ϵ_0. The results shown in figure 7(*a*) indicate that the short-time approximation is uniformly valid for all gap widths at $x = 0$ for drops that are pressed together. For drops that are pulled apart, the short-time approximation eventually breaks down at the centre of the near-contact region. This discrepancy corresponds to the onset of the concentration boundary layer at $x = 0$ which forms at long times according to the analysis presented in Appendix A.

The comparison of the numerical solution with the short-time approximation indicates that at short times, the surfactant distribution is nearly independent of the force parameter, viscosity ratio, and initial gap width. The results shown in figure 7 correspond to viscosity ratio $\lambda = 1$; the short-time approximation is more accurate for smaller values of λ (or smaller initial gap widths) because the short and long time scales are further separated. The accuracy of the short-time approximation is much better for super-critical values of the force parameter $\hat{F} > 1$ or $\hat{F} < 1 - \frac{1}{2}\pi$. For drops that are pushed together by a super-critical force, the entire evolution is accurately described by the short-time approximation. As discussed in § 4.1, the short-time behaviour is characterized by passive convection of the surfactant; deviations of the short-time approximation from the numerical results are a manifestation of surfactant redistribution by Marangoni stresses.

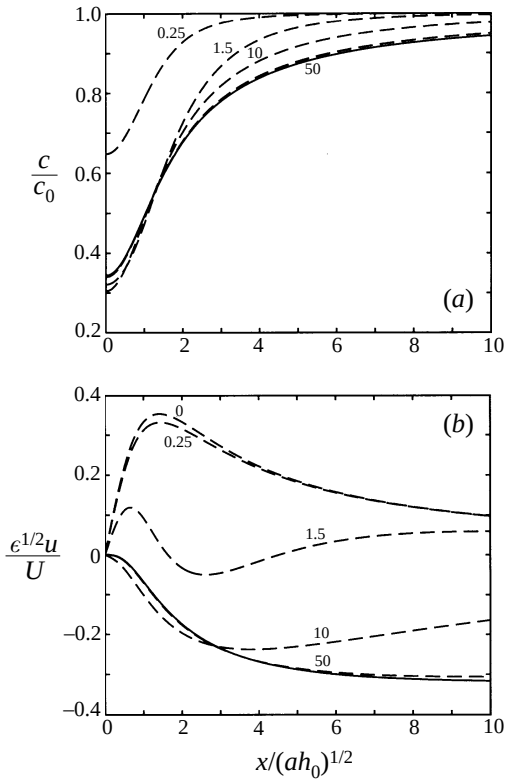

FIGURE 8. Profiles of (*a*) surfactant concentration and (*b*) interfacial velocity at different times t/τ_0 (as labelled) for drops pushed together with $\hat{F} = 0.4$, $\lambda = 1$, $\epsilon_0 = 0.01$ ($\tau_p/\tau_0 = 5.73$), and uniform initial distribution of surfactant: numerical solution (dashed curves), long-time asymptotic solution (solid curves).

5.2.2. *Sub-critical force*

Evolution of the surfactant concentration and interfacial velocity profiles under sub-critical constant force conditions are depicted in figures 8–10. The long-time asymptotic surfactant concentration and interfacial velocity profiles are shown in figures 11 and 12.

Initially, surfactant redistributes on the fast time scale. At $t = 0$, the interfacial velocity is given by formula (3.9). The interfacial velocity profiles shown in figures 8–10 indicate that the velocity remains close to the initial profile for $t < \tau_0$. It follows that the surfactant distribution is accurately described by the short-time approximation. A transition to the long-time behaviour is observed for $t \approx \tau_0$ during which the force balance (4.16) is achieved; the exact time of the transition depends on $\hat{F}$. Thereafter, the long-time similarity solution is attained on the slow time scale τ_p.

The clean spot that forms for subcritical $\hat{F}$ scales with the extent of the lubrication region and therefore shrinks as the gap decreases. Formation of a clean spot is illustrated in figure 9. Fully developed surfactant-free regions are clearly visible in figure 11 for the long-time concentration and velocity profiles corresponding to $\hat{F} > 0.61$.

For all subcritical values of the force parameter, the interfacial velocity is directed

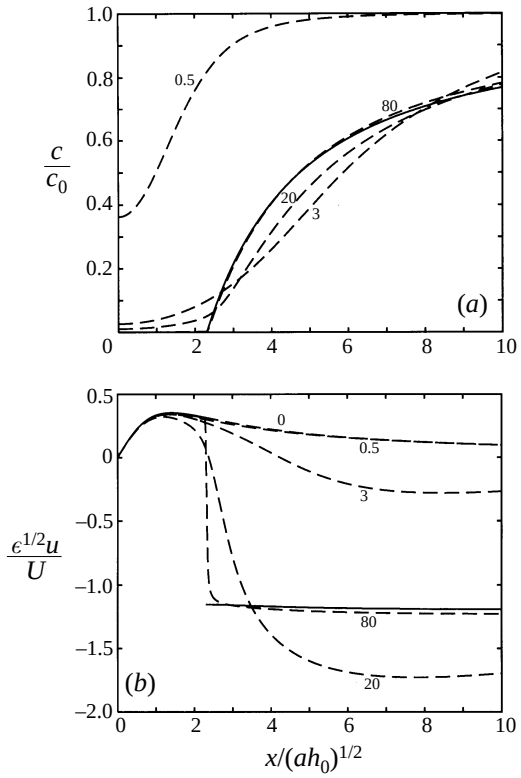

FIGURE 9. Same as figure 8 but for $\hat{F} = 0.9$.

inward at long times except where $c = 0$, as predicted by (4.46) and illustrated by the results shown in figures 8–12. The backflow velocity diverges at the critical values for $\hat{F}$. Where $c = 0$, the velocity is given by (3.9); the discontinuity of u, apparent in figure 9 (*b*), is an artifact of the lubrication approximation.

5.3. *Relaxation*

Figures 13 and 14 show the response of the system to an unsteady external force (4.47) under conditions where the long-time similarity behaviour is established at $t = 0$. The results illustrate the two-time-scale behaviour. The initial relaxation is well described by the short-time approximation: the gap width and surfactant distribution quickly evolve until the force balance (4.50) is approximately established as the results shown in figure 13 indicate. Following the short-time relaxation, the concentration profiles approximately satisfy (4.51). Equilibration of the residual concentration gradients relies on pressure-driven lubrication flow which occurs on the slow time scale. A slow gap width adjustment occurs as the uniform surfactant distribution is gradually attained.

6. Conclusions

A theory has been formulated for near-contact motion of spherical drops with a dilute strongly adsorbed non-diffusing surfactant.

It has been shown that the system evolves on two time scales: a fast time scale τ_0

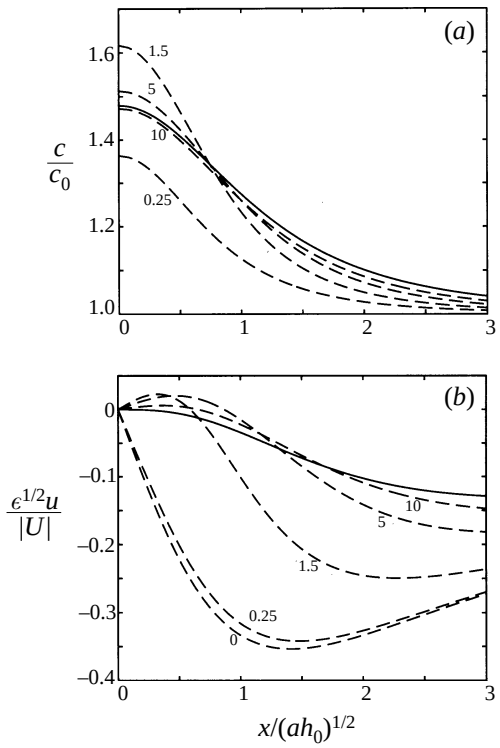

FIGURE 10. Same as figure 8 but for drops pulled apart with $\hat{F} = -0.2$ and $\epsilon_0 = 0.0005$ ($\tau_p/\tau_0 = 25.6$).

characteristic of the near-contact motion between drops with clean interfaces and a slow time scale τ_p associated with rigid particles. Evolution occurs on the fast time scale unless the force F_M generated by Marangoni stresses balances the external force F. On the fast time scale surfactant is passively convected. Marangoni stresses resist the relative motion of the drops but do not appreciably redistribute the surfactant. An analytical solution of the governing equations has been derived for this regime.

The stability of the drops to coalescence is quantitatively characterized by the dimensionless force parameter $\hat{F} = F/(4\pi k T a c_0)$, the external force normalized by Marangoni stresses. For $\hat{F} > 1$ Marangoni stresses cannot balance the external force; thus, drop coalescence occurs on the fast time scale. The coalescence time normalized by τ_0 is independent of the viscosity ratio and initial gap width. The critical value $\hat{F} = 1$ is universal – independent of the viscosity ratio and initial conditions. Drops quickly separate for $\hat{F} < 1 - \frac{1}{2}\pi$. This result is also general except for unusual initial distributions of surfactant.

After the short-time evolution with $1 - \frac{1}{2}\pi < \hat{F} < 1$, the force balance $F_M \approx F$ is achieved at a gap width ϵ_s which depends on the initial distribution of surfactant. Thereafter, the system evolves on the slow time scale towards a long-time similarity solution. The long-time surfactant distribution scales with the extent of the near-contact region; for $1 > \hat{F} > 0.61$, a shrinking surfactant-free clean spot forms. At long times, surface backflow slows the approach of the drops and accelerates their separation compared to the relative velocity of rigid particles. For drops pressed

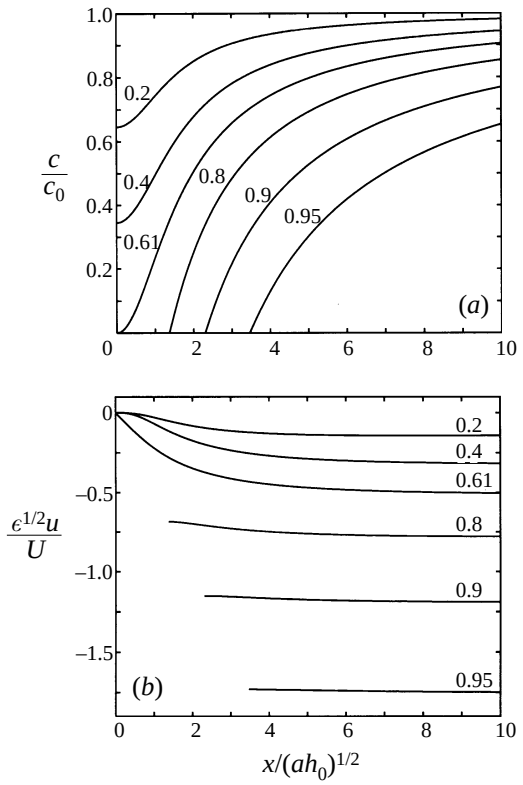

FIGURE 11. Long-time similarity profiles of (*a*) surfactant concentration and (*b*) interfacial velocity for drops that are pushed together with different values of $\hat{F}$ (as labelled). For a clean spot, interfacial velocity is given by (3.9).

together by a subcritical force the gap drains exponentially at long times; coalescence does not occur. A sharp stability transition is predicted for $\hat{F} = 1$.

Van der Waals attraction reduces the critical force parameter and blurs the stability transition for coalescence. Equating van der Waals attraction to the external force yields a characteristic gap width

$$\epsilon_A = \left(\frac{A}{6Fa}\right)^{1/2} \tag{6.1}$$

for the range of van der Waals attraction, where A is the Hamaker constant; rapid coalescence occurs for $\epsilon_A > \epsilon_s$. According to (4.16), an estimate of the critical force parameter for coalescence is

$$\hat{F} = \hat{F}_{MS}(\epsilon_A), \tag{6.2}$$

where F_{MS} depends on the initial distribution of surfactant. Adsorbed surfactant may modify the van der Waals attraction between drops. Under these conditions, the surfactant distribution calculated herein can be used to compute the attractive force.

Surfactant-covered drops have an elastic response to unsteady external forces because of energy stored in the surfactant distribution. For short-time displacements from a uniform distribution of surfactant, the behaviour is analogous to a damped nonlinear spring; generally, an irreversible two-time-scale relaxation process is ob-

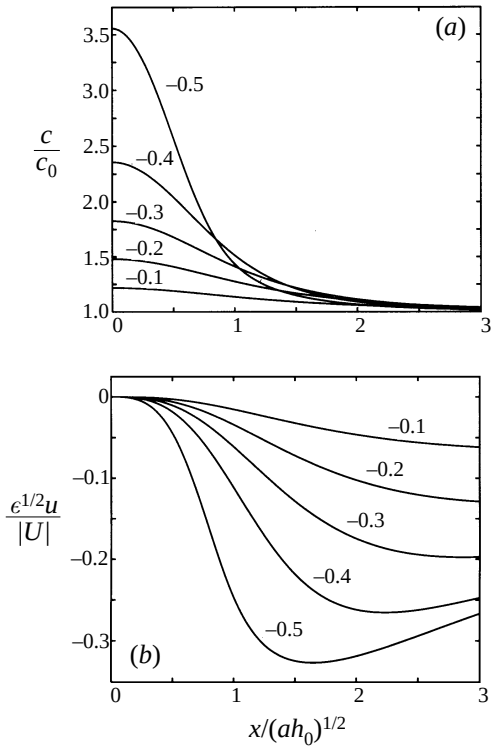

FIGURE 12. Same as figure 11 but for drops that are pulled apart.

served. For near-critical external forces, the stable long-time behaviour of surfactant-covered drops is very sensitive to force fluctuations.

In general, the initial and boundary conditions for the lubrication description presented herein must be supplied by a separate calculation for the outer flow. The evolution preceding the lubrication regime may establish the long-time behaviour at much larger gap widths than predicted by calculations that suppose a uniform initial distribution of surfactant in the near-contact region. Boundary integral calculations indicate that this occurs (Papadopoulos, Bławzdziewicz & Loewenberg 1996).

Surface diffusion, neglected herein, may significantly affect the behaviour of surfactant-covered drops at long times and small gaps. For $\hat{F} < 1$, surface diffusion provides a lubrication cutoff so that coalescence can occur in the absence of van der Waals attraction (Bławzdziewicz, Wajnryb & Loewenberg 1998).

Drop deformation is important for larger drops and higher surfactant concentrations. Currently, calculations are underway to explore the near-contact motion of surfactant-covered deformable drops (Papadopoulos *et al.* 1996).

The analysis presented herein is valid to $\epsilon^{1/2} \ll \lambda \ll \epsilon^{-1/2}$. An extension to highly viscous drops $\lambda \geqslant O(\epsilon^{-1/2})$ is possible following the more general numerical method of Davis *et al.* (1989). Accordingly, the flow field inside the drops is described by a boundary integral formulation. These calculations would yield an $O(\epsilon^{1/2})$ correction to our results for $\lambda = O(1)$. Surfactant effects are less pronounced for $\lambda = O(\epsilon^{-1/2})$ because Marangoni stresses are comparable to viscous stresses generated by flow within the drops and low interfacial mobility hinders surfactant redistribution. In this regime, the system evolves on a single time scale because $\tau_0 \approx \tau_p$.

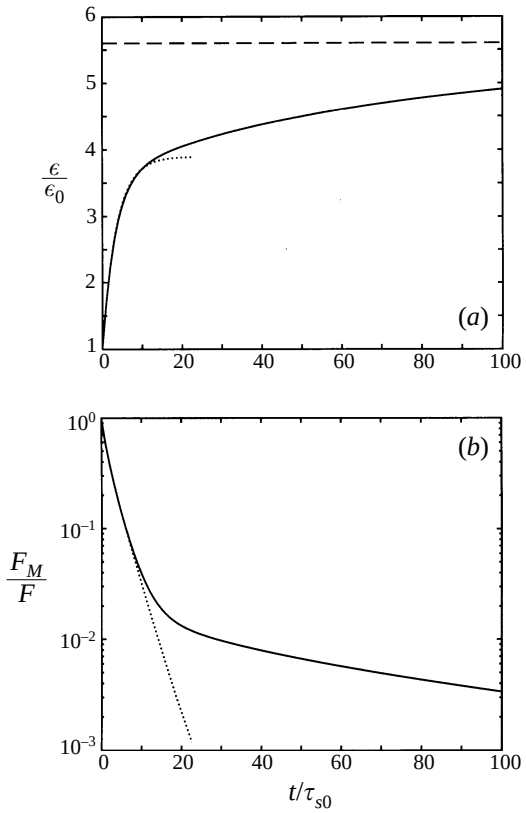

FIGURE 13. Relaxation from long-time similarity solution with $\hat{F} = 0.4$, $\epsilon_0 = 0.0005$, and $\lambda = 1$ ($\tau_{sp}/\tau_{s0} = 25.6$), (*a*) gap width, (*b*) force generated by Marangoni stresses: numerical solution (solid curves), short-time approximation (dotted curves), final gap width (dashed line).

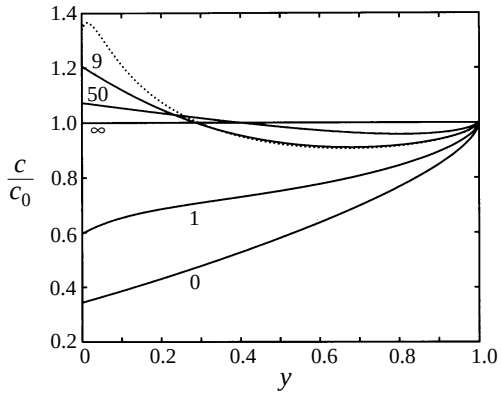

FIGURE 14. Surfactant concentration profiles corresponding to conditions in figure 13 at different times t/τ_{s0} (as labelled). Numerical solution (solid curves), short-time approximation for $\epsilon = \epsilon_s$ (dotted curve).

Experimental studies are unavailable for a quantitative comparison to the predictions presented in this article. A concentrated emulsion of closely packed spherical drops under centrifugation should provide a suitable experimental system for testing the stability predictions of our analysis for a uniform initial distribution of surfactant.

This work was supported by NSF grant CTS-9624615 and NASA grant NAG3-1935.

Appendix A. Similarity solution for separating drops with near-critical pulling force

According to (4.26), $C(y)$ is everywhere negative for $\hat{F} < 0$. We seek an asymptotic solution of (4.27) for $|C(0)| \ll 1$ with $\hat{F} < 0$. Given (4.29) and (4.45) it follows that $|C(y)|$ is everywhere small.

Inspection of (4.27) reveals that the nonlinear term is unimportant except for $\tilde{y} = y/|C(0)| = O(1)$. An asymptotic solution $C(y)$ was found by matching an outer expansion

$$f(y) = |C(0)|^{1/2} f_0(y) + |C(0)|^2 f_1(y) + O(|C(0)|)^{7/2}, \quad y \gg |C(0)|, \tag{A 1}$$

to an expansion for the inner region

$$f(y) = \tilde{f}_0(\tilde{y}) + |C(0)|\tilde{f}_1(\tilde{y}) + O(|C(0)|)^2, \quad \tilde{y} = O(1), \tag{A 2}$$

where

$$f(y) = C(y)/C(0). \tag{A 3}$$

Inserting the outer expansion (A 1) into (4.27) and solving the resulting linear equations, we obtain

$$f_0 = \frac{a_0}{[y(2-y)]^{1/2}}, \tag{A 4}$$

$$f_1 = \frac{2a_0^2}{15} \frac{10 - 35y + 30y^2 - 10y^3 + 2y^4}{(2-y)^3 y^2}, \tag{A 5}$$

where a_0 is a constant. At leading order, the outer solution coincides with the short-time solution (4.2) for large displacements $\epsilon/\epsilon_0 \gg 1$ of the separating drops.

In terms of the inner variable (4.27) becomes

$$\tilde{y}\frac{\mathrm{d}f}{\mathrm{d}\tilde{y}} + \left(1 - |C(0)|\,\tilde{y}\right)\left[\frac{\mathrm{d}}{\mathrm{d}\tilde{y}}(\tilde{y}f) + \frac{\mathrm{d}}{\mathrm{d}\tilde{y}}\left(\tilde{y}\frac{\mathrm{d}}{\mathrm{d}\tilde{y}}f^2\right)\right] = 0. \tag{A 6}$$

Inserting (A 2) into (A 6), expanding the solution for $\tilde{y} \to \infty$, and matching to the outer expansion for $y \to 0$ we obtain

$$\tilde{f}_0 = \frac{a_0}{(2\tilde{y})^{1/2}} + \frac{a_0^2}{6\tilde{y}^2} + O(1/\tilde{y}^{7/2}), \tag{A 7}$$

$$\tilde{f}_1 = \frac{a_0}{4}\left(\frac{\tilde{y}}{2}\right)^{1/2} - \frac{a_0^2}{3\tilde{y}} + O(1/\tilde{y}^{5/2}), \tag{A 8}$$

where $\tilde{f}_0(0) = 1$, $\tilde{f}_0'(0) = \frac{1}{2}$ and $\tilde{f}_1(0) = \tilde{f}_1'(0) = 0$. In writing, (A 8) we have assumed that the $O(\tilde{y}^{-1/2})$ term associated with the homogeneous solution of (A 6) at first-order is absent from the solution. This assumption is supported by our numerical calculations as explained below. Numerical integration of the leading-order inner equation yields

$$a_0 = 0.6334. \tag{A 9}$$

From (A 1) and (A 4), we have

$$C(1) = -a_0\,|C(0)|^{3/2} + O(|C(0)|^3), \tag{A 10}$$

From (4.17) and (A 3), we have

$$\hat{F} = 1 - \frac{C(0)}{C(1)} \int_0^1 f(y)\,\mathrm{d}y. \tag{A 11}$$

which, with the help of (A 4) and (A 10), can be rewritten as

$$\hat{F} = 1 - \tfrac{1}{2}\pi + \Delta\hat{F}, \tag{A 12}$$

where

$$\Delta\hat{F} = -\frac{1}{a_0} \int_0^1 \left[|C(0)|^{-1/2} f(y) - f_0(y)\right]\,\mathrm{d}y. \tag{A 13}$$

By expanding

$$f_0 = \frac{a_0}{(2y)^{1/2}} \left[1 + \frac{y}{4} + O(y^2)\right], \quad y \to 0, \tag{A 14}$$

and inserting (A 1) and (A 2) into (A 13) we obtain

$$\Delta\hat{F} = -\frac{|C(0)|^{1/2}}{a_0} \left\{ \int_0^{\tilde{y}^*} \left(\tilde{f}_0 - \frac{a_0}{2\tilde{y})^{1/2}} \right) \mathrm{d}\tilde{y} \right.$$
$$\left. + |C(0)| \left[\int_0^{\tilde{y}^*} \left(\tilde{f}_1 - \frac{a_0}{4} \left(\frac{\tilde{y}}{2} \right)^{1/2} \right) \mathrm{d}\tilde{y} + \int_{y^*}^1 f_1 \mathrm{d}y \right] \right\} + o\left(|C(0)|^{3/2}\right), \tag{A 15}$$

where $|C(0)| \ll y^* \ll 1$ and $\tilde{y}^* = y^*/|C(0)|$.

At zeroth order, (A 6) is integrated to yield

$$\int_0^{\tilde{y}^*} \tilde{f}_0\,\mathrm{d}\tilde{y} = \tilde{y}^* \left[2f_0(\tilde{y}^*) + \frac{\mathrm{d}}{\mathrm{d}\tilde{y}^*} f_0^2(\tilde{y}^*) \right], \tag{A 16}$$

which, combined with (A 7), gives

$$\int_0^{\tilde{y}^*} \left(\tilde{f}_0 - \frac{a_0}{(2\tilde{y})^{1/2}} \right) \mathrm{d}\tilde{y} = -|C(0)| \frac{a_0^2}{6y^*} + O\left(|C(0)|/y^*\right)^{5/2}. \tag{A 17}$$

By integrating (A 5) and (A 8) we obtain

$$\int_{y^*}^1 f_1\,\mathrm{d}y = a_0^2 \left(\frac{1}{6y^*} + \tfrac{1}{3}\log y^* + \mathrm{const} \right) + O(y^*), \tag{A 18}$$

$$\int_0^{\tilde{y}^*} \left[\tilde{f}_1 - \frac{a_0}{4} \left(\frac{\tilde{y}}{2} \right)^{1/2} \right] \mathrm{d}\tilde{y} = -\frac{a_0^2}{3} \log\left(y^*/|C(0)|\right) + \mathrm{const} + O\left(|C(0)|/y^*\right)^{3/2}. \tag{A 19}$$

Inserting (A 17)–(A 19) into (A 15) yields

$$\Delta\hat{F} = |C(0)|^{3/2} \left(-\frac{a_0}{3} \log|C(0)| + b \right) + o\left(|C(0)|^{3/2}\right), \tag{A 20}$$

where a_0 is given by (A 9) and, by comparing (A 20) to the numerically obtained similarity solution,

$$b = 0.5953. \tag{A 21}$$

The inverse relation

$$|C(0)|^{3/2} = f_s(\Delta\hat{F}) \tag{A 22}$$

can be obtained by solving (A 20) iteratively; the first iteration yields

$$f_s(\Delta\hat{F}) = \frac{\Delta\hat{F}}{-\frac{2}{9}a_0 \log \Delta\hat{F} + b}. \tag{A 23}$$

Accurate convergence is obtained with several iterations. The results indicate that $|C(0)| = 0$ for $\Delta\hat{F} = 0$.

A similar analysis can be applied to (4.54) in the case when $\bar{c}(y)$ is described by the long-time similarity solution for the near critical pulling force. From (4.54), (A 3), (A 10), and the relation

$$\int_0^1 [1 - 2(1-y)^2]\, f_0(y)\, \mathrm{d}y = 0 \tag{A 24}$$

we obtain

$$-\epsilon_0 \frac{\delta\hat{F}}{\delta\epsilon} = \frac{1}{a_0}\int_0^1 [1 - 2(1-y)^2]\ \left[|C(0)|^{-1/2} f(y) - f_0(y)\right]\ \mathrm{d}y. \tag{A 25}$$

This relation is decomposed into a sum of integrals over the inner and the outer regions, in analogy to the decomposition (A 15). The expansions (A 1) and (A 2) with (A 4)–(A 5) and (A 7)–(A 8) are used to evaluate the integrals. Combining the leading-order results yields

$$-\epsilon_0 \frac{\delta\hat{F}}{\delta\epsilon} = |C(0)|^{3/2}\left(-a_0 \log|C(0)| + b_1\right) + o\left(|C(0)|^{3/2}\right), \tag{A 26}$$

where a_0 is given by (A 9) and, by comparing formula (A 26) to the numerically obtained similarity solution,

$$b_1 = 0.8986. \tag{A 27}$$

An $O(\tilde{y}^{-1/2})$ term in (A 8) would generate an $O(|C(0)|)$ terms in (A 20) and (A 26) which is inconsistent with our numerical calculations. In principle, a detailed analysis of the first-order solution of (A 6) could be used to rigorously justify the absence of this term in (A 8).

Appendix B. Two-point approximations

Consider a function $q(\hat{F})$ which is regular at $\hat{F} = 0$ and has a known singularity $q_s(\hat{F})$ at $\hat{F} = 1 - \frac{1}{2}\pi$. The relative particle velocity $\bar{U}$ and the concentration at the centre of the near-contact region $\bar{c}(0)$ in a state described by the similarity solution are examples of such functions. Another example is the quantity $-\epsilon_0^{-1}\delta\epsilon/\delta\hat{F}$, describing the response of the similarity solution to fluctuations of the external force.

The two-point approximation

$$q(\hat{F}) \approx q_s(\hat{F}) + \sum_{i=0}^{n} \left[q^{(i)}(0) - q_s^{(i)}(0)\right] \frac{\hat{F}^i}{i!}, \tag{B 1}$$

where the superscript (i) denotes the ith derivative with respect to $\hat{F}$, has a correct asymptotic behaviour at $\hat{F} = 1 - \frac{1}{2}\pi$ and correct first n derivatives at $\hat{F} = 0$. Often approximation (B 1) has much better global accuracy than the asymptotic expression $q_s(\hat{F})$ or the truncated Taylor series expansion of $q(\hat{F})$.

With the help of the expansions (4.35) and (4.40) the approximation (B 1) with $n = 1$ can be explicitly constructed for $\bar{U}$ and with the help of the expansions (4.36) and

(4.42) for $\bar{c}$. For $-\epsilon_0^{-1}\delta\epsilon/\delta\hat{F}$, the approximation (B 1) with $n = 2$ can be obtained from (4.55) and (4.57). As illustrated in figures 5 and 6 the approximations are accurate for all negative subcritical values of $\hat{F}$ and for moderate positive values $\hat{F}$.

REFERENCES

Bławzdziewicz, J., Wajnryb, E. & Loewenberg, M. 1998 Hydrodynamic interactions and collision efficiencies of surfactant-covered spherical drops: Incompressible surfactant. *J. Fluid Mech.* (submitted).

Davis, R. H., Schonberg, J. A. & Rallison, J. M. 1989 The lubrication force between two viscous drops. *Phys. Fluids* **1**, 77–81.

Edwards, D. A., Brenner, H. & Wasan, D. T. 1991 *Interfacial Transport Processes and Rheology*. Butterworth-Heinemann.

Hall, G. & Watt, J. M. (Eds.) 1976 *Modern Numerical Methods for Ordinary Differential Equations*. Clarendon.

Hodgson, T. D. & Lee, J. C. 1969 The effect of surfactants on the coalescence of a drop at an interface I. *J. Colloid Interface* **30**, 94–108.

Ivanov, I. 1988 *Thin Liquid Films*. Marcel Dekker.

Kim, S. & Karrila, S. J. 1991 *Microhydrodynamics*. Butterworth-Heinemann.

Kralchevsky, P. A., Danov, K. D. & Ivanov, I. B. 1996 Thin liquid film physics. In *Foams* (ed. R. K. Prud'homme & S. A. Khan), pp. 1–98. Marcel Dekker.

Levich, V. G. 1962 *Physicochemical Hydrodynamics*. Prentice–Hall.

Li, X. & Pozrikidis, C. 1997 The effect of surfactants on drop deformation and on the rheology of dilute emulsions in Stokes flow. *J. Fluid Mech.* **341**, 165–194.

Maldarelli, C. & Huang, W. 1996 The effect of surfactants on the motion of bubbles and drops. In *Flow of Particles in Suspensions* (ed. U. Schaflinger), pp. 125–160. CISM Courses and Lectures No. 370, Springer.

Pal, R. 1993 Rheological behaviour of surfactant-flocculated water-in-oil emulsions. *Colloids Surfaces* A **71**, 173–185.

Papadopoulos, D., Bławzdziewicz, J. & Loewenberg, M. 1996 Near-contact motion and coalescence of deformable drops. Presented at Annual AIChE Meeting, Chicago.

Pawar, Y. & Stebe, K. J. 1996 Marangoni effects on drop deformation in an extensional flow: the role of surfactant physical chemistry I. Insoluble surfactants. *Phys. Fluids* **8**, 1–14.

Russel, W. B., Saville, D. A. & Schowalter, W. R. 1989 *Colloidal Dispersions*. Cambridge University Press.

Stone, H. A. & Leal, L. G. 1990 The effects of surfactants on drop deformation and breakup. *J. Fluid Mech.* **220**, 161–186.

Yiantsios, S. G. & Davis, R. H. 1991 Close approach and deformation of two viscous drops due to gravity and van der Waals forces. *J. Colloid Interface Sci.* **144**, 412–433.

Zinchenko, A. Z. 1982 Calculation of close interaction between two drops, with internal circulation and slip effect taken into account. *Prikl. Mat. Mekh.* **45**, 564–567.